Cell

A Subpopulation of Adult Skeletal Muscle Stem Cells Retains All Template DNA Strands after Cell Division

Pierre Rocheteau,[1] Barbara Gayraud-Morel,[1] Irene Siegl-Cachedenier,[2,3] Maria A. Blasco,[2] and Shahragim Tajbakhsh[1,*]
[1]Institut Pasteur, Stem Cells and Development, Department of Developmental Biology, CNRS URA 2578, 25 rue du Dr. Roux, Paris 75015, France
[2]Telomeres and Telomerase Group, Molecular Oncology Programme, Spanish National Cancer Centre (CNIO), Melchor Fernández Almagro 3, 28029 Madrid, Spain
[3]Present address: Department of Genetic Medicine and Development, University of Geneva Medical School, C.M.U., 1 rue Michel Servet, 1211 Geneva 4, Switzerland
*Correspondence: shaht@pasteur.fr
DOI 10.1016/j.cell.2011.11.049

SUMMARY

Satellite cells are adult skeletal muscle stem cells that are quiescent and constitute a poorly defined heterogeneous population. Using transgenic *Tg:Pax7-nGFP* mice, we show that Pax7-nGFP^{Hi} cells are less primed for commitment and have a lower metabolic status and delayed first mitosis compared to Pax7-nGFP^{Lo} cells. Pax7-nGFP^{Hi} can give rise to Pax7-nGFP^{Lo} cells after serial transplantations. Proliferating Pax7-nGFP^{Hi} cells exhibit lower metabolic activity, and the majority performs asymmetric DNA segregation during cell division, wherein daughter cells retaining template DNA strands express stem cell markers. Using chromosome orientation-fluorescence in situ hybridization, we demonstrate that all chromatids segregate asymmetrically, whereas Pax7-nGFP^{Lo} cells perform random DNA segregation. Therefore, quiescent Pax7-nGFP^{Hi} cells represent a reversible dormant stem cell state, and during muscle regeneration, Pax7-nGFP^{Hi} cells generate distinct daughter cell fates by asymmetrically segregating template DNA strands to the stem cell. These findings provide major insights into the biology of stem cells that segregate DNA asymmetrically.

INTRODUCTION

Subcellular constituents including misfolded proteins, centrosomes, and transcripts can segregate asymmetrically during cell division and also influence the fate of daughter cells (Macara and Mili, 2008; Neumüller and Knoblich, 2009; Tajbakhsh and Gonzalez, 2009). Arguably the most perplexing is the asymmetric segregation of DNA. In the bacteria *Escherichia coli*, leading and lagging DNA strands of a replication fork were reported to segregate to different subcellular locations (White et al., 2008); similarly, replication origins move toward opposite ends of the cell in *Caulobacter crescentus* (Bowman et al., 2008). In metazoans, studies involving a pulse with thymidine nucleotide analogs, followed by a chase, identified label-retaining cells (LRCs) in culture or in stem cells in vivo suggesting the occurrence of template DNA strand segregation (TDSS; see Rando, 2007; Tajbakhsh and Gonzalez, 2009). Some of these observations led to the "immortal DNA strands" hypothesis that postulated that stem cells retain old DNA strands of all chromosomes in the longer-lasting daughter stem cell, thereby avoiding a mutation load potentially arising from DNA replication. This model presumes that stem cells perform consecutive asymmetric divisions invariantly, with little to no intervening symmetric cell divisions, that sister chromatid exchange does not occur, and that excision and repair modes of DNA repair are minimal in stem cells (Cairns, 2006; Lansdorp, 2007; Rando, 2007; Tajbakhsh, 2008). However, most of these issues remain largely untested. In addition, reports in support or against biased DNA segregation for the same tissue (Escobar et al., 2011; Falconer et al., 2010; Potten et al., 2002; Quyn et al., 2010; Schepers et al., 2011) have generated considerable debate (Lansdorp, 2007; Tajbakhsh, 2008). Currently, it is difficult to determine when biased DNA segregation occurs and how this is related to the fate of stem cells, due largely to the lack of information on the biology of these stem cells and the inability to isolate them prospectively.

The regulation of gene expression might be one consequence of TDSS, whereby individual alleles, or chromatids, would be maintained either as silent or permissive for gene expression; however, these notions also remain unproven (Klar, 1994; Lansdorp, 2007). Recent studies reported that not all chromatids participate in biased DNA segregation, in differentiating ES cells (Armakolas and Klar, 2006), and cells in the intestinal crypt (Falconer et al., 2010), suggesting that investigation of the occurrence of nonrandom DNA segregation requires analysis of single chromatids.

Satellite cells ensure muscle growth and repair during postnatal development, and after muscle damage they effect tissue

repair (Tajbakhsh, 2009; Zammit et al., 2006). After skeletal muscle injury, these quiescent stem cells in the adult enter the cell cycle and generate myoblasts that will fuse to form myofibers. Eventually, satellite cells replenish the niche as regeneration is achieved. Muscle stem cell self-renewal has been demonstrated up to several rounds after muscle injury and by the transplantation of satellite cells associated with myofibers (Collins et al., 2005; Hall et al., 2010; Kitamoto and Hanaoka, 2010; Montarras et al., 2005; Sacco et al., 2008), but unlike the blood and skin, serial transplantations have not been reported for purified satellite cells; therefore, their long-term self-renewal capacity has not been evaluated.

Compelling evidence points to heterogeneity among quiescent muscle stem cells, regarding their gene expression signature and their functional properties (Biressi et al., 2007; Kuang et al., 2007; Kuang and Rudnicki, 2008; Shinin et al., 2006; Tajbakhsh, 2009). Satellite cells express the paired/homeodomain gene *Pax7*, which plays a critical role in satellite cell maintenance during perinatal life, but it is dispensable in the adult (Kuang et al., 2006; Lepper et al., 2009; Oustanina et al., 2004; Relaix et al., 2006; Seale et al., 2000). The myogenic regulatory genes *Myf5* and *Myod* play key roles in determining muscle cell fate; Myf5 protein is expressed in most quiescent satellite cells (Gayraud-Morel et al., 2012), whereas Myod protein is a hallmark of the activated cell state once satellite cells re-enter the cell cycle. A third myogenic regulatory factor Myogenin is expressed in cells undergoing differentiation (Tajbakhsh, 2009; Zammit et al., 2006). We showed previously that a subpopulation of satellite cells performs TDSS using the thymidine analog 5-bromo-2′-deoxyuridine (BrdU), whereby cells retaining template DNA strands expressed the upstream marker Pax7 (Shinin et al., 2006). Another study reported TDSS in satellite cells using the analogs CldU and IdU (Conboy et al., 2007). It is not clear, however, if all or only a subset of satellite cells has the potential to perform TDSS, how many chromosomes are involved in this process, and what are the properties of these cells.

We used a transgenic *Tg:Pax7-nGFP* mouse that marks all satellite cells to identify a reversible dormant cell state in the Pax7^{Hi} quiescent subpopulation and show by serial transplantations that these cells self-renew and give rise to myogenic cells that are more primed for commitment. Furthermore, the majority of cycling Pax7^{Hi} cells reproducibly performs biased DNA segregation, and analysis by chromosome orientation-fluorescence in situ hybridization (CO-FISH) demonstrates that this process involves essentially all chromatids.

RESULTS

Label Retention and Relative *Pax7* Expression Identify a Subpopulation of Dormant Adult Muscle Stem Cells

Pulse-chase experiments using thymidine analogs have been used to identify stem cells and their niche based on the assumption that they divide more slowly than their committed daughter cells (Fuchs et al., 2004; Li and Clevers, 2010). We showed previously, by pulse-chase labeling, that LRCs are present in the skeletal muscle niche after 10 weeks of chase and that TDSS occurs in a subpopulation of satellite cells (Shinin et al., 2006). We used a similar strategy under two different paradigms (growth and injury) to investigate further this property using *Tg: Pax7-nGFP* mice that identify all satellite cells in adult mice (Figures 1A–1C; Sambasivan et al., 2009) and, thus, allow their prospective isolation by fluorescence-activated cell sorting (FACS, Figure 1D). For postnatal day (P) growth, *Tg: Pax7-nGFP* mice were injected intraperitoneally with BrdU for 5 days (P3–P7) when the majority of myogenic cells are proliferating (Figure 1E). After the last injection (T0; P7), the majority of the cells (>95%) were saturated with BrdU, and by 11.5 weeks, 6.3% ± 1.4% of the cells continued to retain robust label (Figures 1F–1J).

We reasoned that muscle stem cell heterogeneity might be correlated with the expression level of the upstream marker *Pax7.* Two subpopulations were isolated by FACS at opposite ends of the spectrum of green fluorescent protein (GFP) expression levels. These were designated as Pax7-nGFP^{Hi} and Pax7-nGFP^{Lo}, and they each corresponded to ~10% of the total population (Figure 1D). Interestingly, about 2-fold more LRCs were observed in the Pax7-nGFP^{Hi} subpopulation compared to Pax7-nGFP^{Lo} fraction at all time points examined (Figure 1F histograms; 11.5 weeks chase 10.41% LRC in Pax7-nGFP^{Hi}, 5.1% in Pax7-nGFP^{Lo}). To examine the commitment status of these subpopulations, quiescent muscle stem cells were isolated by FACS, and mRNA was extracted for comparative gene expression. Notably, RT-qPCR showed higher levels of *Pax7* transcripts in Pax7-nGFP^{Hi} cells, indicating that GFP expression reflects endogenous *Pax7* expression quantitatively (Figure 1K). This was confirmed by western blot wherein Pax7-nGFP^{Hi} cells expressed more Pax7 protein (Figure 1L). *CXCR4* and *CD34*, which were reported to be markers of stemness (Beauchamp et al., 2000; Sherwood et al., 2004), were also upregulated in Pax7-nGFP^{Hi} cells (Figures 1K and 1M), whereas the expression of *Sca1* and *Desmin*, which are associated with myogenic commitment (Kuang and Rudnicki, 2008), were reduced (Figure 1K). Consistent with their commitment status, significantly lower levels of transcripts were observed for the differentiation gene *Myogenin* in Pax7-nGFP^{Hi} compared to Pax7-nGFP^{Lo} cells (Figure 1K).

The behavior of satellite cells was then investigated by live video microscopy immediately after their isolation and culture. Pax7-nGFP^{Hi} entered the cell cycle and took a longer time to divide compared to Pax7-nGFP^{Lo} cells for the first division (mean time: 33 versus 25.5 hr, respectively, n = 200 cells for each; Figure 2A; see Movies S1 and S2 available online). Notably, however, no differences in cell-cycle time were observed for subsequent divisions (every 10 hr, n = 200 cells; Movie S3). The delay in cell-cycle entry was confirmed in vivo using pulsed injections of the nucleotide analog EdU after muscle injury (Figure 2B). Because Pax7-nGFP^{Hi} quiescent stem cells have a higher percentage of LRCs, and they take longer to perform the first cell division after activation, we reasoned that this subpopulation was in a more dormant state (i.e., lower metabolism). Interestingly, higher levels of active mitochondria, as measured by MitoTracker fluorescence intensity (Figure 2C), and higher levels of ATP (Figure 2D) were observed in the Pax7-nGFP^{Lo} cells. Metabolic demands correlate with oxidative capacity and mitochondrial DNA (Moyes and Battersby, 1998). Accordingly, RT-qPCR of mitochondrial transcription factor A (Tfam; Garstka et al., 2003) and mitochondrial-specific polymerase γ (catalytic

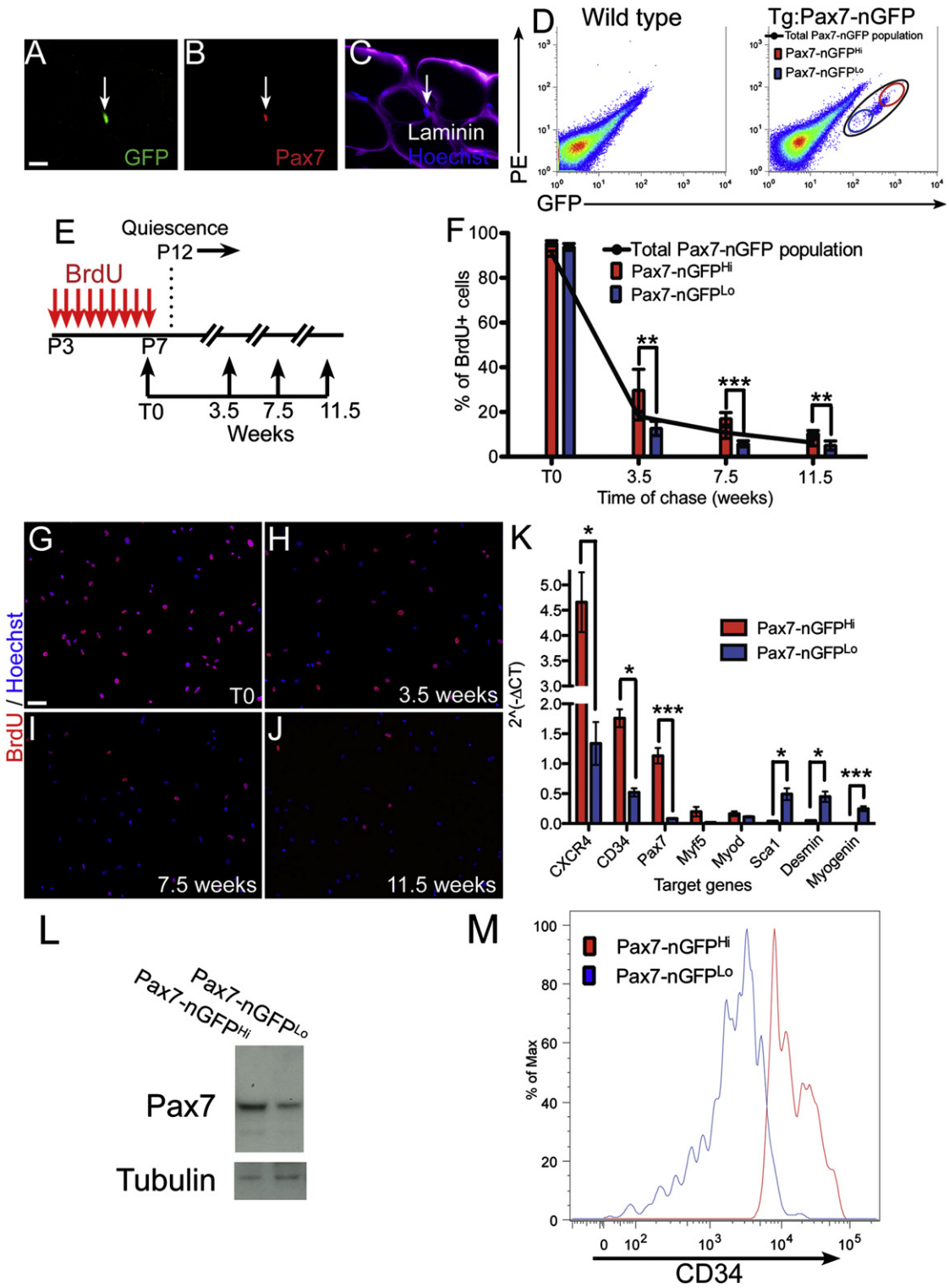

Figure 1. Level of Pax7-nGFP Expression Reflects Muscle Stem Cell Heterogeneity

(A–C) Transverse section of Tibialis anterior (TA) muscle of *Tg:Pax7-nGFP* mouse; arrows indicate satellite cell with coexpression of nGFP and Pax7 (n = 795 nuclei; TA of n = 4 animals).

(D) FACS profile of wild-type (left panel) and Pax7-nGFP mouse (right panel). Gating for Pax7-nGFP^{Hi} and Pax7-nGFP^{Lo} is indicated within total nGFP population. GFP, GFP (488 channel); PE, Phycoerythrin (594 channel). Color on profile indicates cell density: blue, low cell density; red, high cell density.

(E) Scheme of BrdU injections during perinatal growth.

PolG, and accessory PolG2) was upregulated in Pax7-nGFP^{Lo} cells (Figure 2E), indicating a higher energetic demand.

Although both quiescent subpopulations were negative for Myod protein, which marks activated satellite cells, shortly after their isolation, Myod protein was detected in virtually all of the Pax7-nGFP^{Lo} cells after an overnight in culture, whereas only 39% of Pax7-nGFP^{Hi} cells were Myod positive (Figures 2F–2L). In agreement with these observations, 35.2% of Pax7-nGFP^{Hi} and 98.18% of Pax7-nGFP^{Lo} activated satellite cells were positive for Myod protein 18 hr postinjury of muscle in vivo (prior to the first mitosis, Figure 2L). At 48 hr postinjury, or after 2 days in culture, virtually all of the cells were positive for Myod (Figure 2L). Analysis by live video microscopy did not show cell death in these subpopulations. In keeping with these findings, clonal analysis of the two subpopulations (~90 clones each, n = 3 mice; data not shown) showed that Myogenin (5.02% ± 0.90% Pax7-nGFP^{Hi}, 72.26% ± 3.06% Pax7-nGFP^{Lo}, day 3 in culture; n = 3 mice) and myotube formation was delayed in Pax7-nGFP^{Hi} cells. After 2 weeks in culture, both populations generated similar numbers of progeny cells (~1,209 ± 162 cells/clone, n = 3 mice; data not shown). Taken together, these findings indicate that Pax7-nGFP^{Hi} cells represent a distinguishable phenotypic cell state, one that is more dormant and less primed for myogenic commitment than Pax7-nGFP^{Lo} cells.

Self-Renewal and Differentiation Potential of Serially Transplanted Subpopulations of Satellite Cells

To assess the functional properties of satellite cells, we performed serial passages and FACS analysis of each subpopulation in vitro and in vivo. Interestingly, in all cases in culture, only Pax7-nGFP^{Hi} cells replenished the total GFP^{+} pool (total three passages), whereas Pax7-nGFP^{Lo} failed to replenish the GFP^{+} myogenic population (Figures 3A and 3Ba–3Bi; n = 3 mice). We then examined the differentiation and self-renewal potential of these subpopulations in transplantation and regeneration assays. Two transgenic mice were used for quantifications: *Tg:CAG-hPLAP* carrying the human placental alkaline phosphatase gene that is expressed ubiquitously (DePrimo et al., 1996), and *Tg:MLC3F-nlacZ-2E* that marks differentiated myonuclei (Kelly et al., 1995). Pax7-nGFP^{Hi}/T ("T" is the abbreviation for triple transgenic) and Pax7-nGFP^{Lo}/T were isolated by FACS, and 10,000 GFP^{+} cells were transplanted in cryodamaged TA muscle of immunocompromised *Rag2*$^{-/-}$*:*$\gamma C^{-/-}$ mice. Four weeks later, analysis by immunofluorescence showed a large area of newly generated PLAP^{+} myofibers and self-renewed satellite cells surrounded by a Laminin^{+} basement membrane, with both subpopulations (Figures 3Ca–3Cd, 3E, and 3F). The renewed satellite cells were quiescent as assessed by lack of expression of the cell-cycle marker Ki67 (Figures 3Da–3Dd).

To assess the long-term regenerative capacity of the muscle stem cell subpopulations in vivo, an initial transplantation was performed with 10000 Pax7-nGFP^{Hi} and Pax7-nGFP^{Lo} quiescent satellite cells isolated by FACS (Figure 3G). Three weeks later, several thousand GFP^{+} satellite cells were collected, pooled for each subpopulation, and used to transplant into the preinjured Tibialis anterior muscle of secondary recipient mice. Subsequent serial transplantations were performed in a similar manner (seven rounds maximum; Figure 3G). To determine if all transplanted cells were participating actively and entered the cell cycle, 24 hr posttransplantation, BrdU was injected for 4 days, and the mice were sacrificed for analysis. All GFP^{+} satellite cells were BrdU^{+} (data not shown). A drop in cell numbers was often observed between transplanted and harvested cells, likely due to cell death immediately after transplantation (Beauchamp et al., 1999; Gayraud-Morel et al., 2009). Notably, however, in some cases, up to 35 times more GFP^{+} cells were collected than were injected initially (e.g., fifth transplantation; Figure 3G). In some experiments, transplanted muscles were stained for X-gal or PLAP to demonstrate the regenerative capacity of the donor cells (Figure 3H). In accordance with in vitro results (Figure 3B), in two of five rounds of independent serial transplantation experiments, only the Pax7-nGFP^{Hi}/T subpopulation yielded Pax7-nGFP^{Hi} cells, whereas the Pax7-nGFP^{Hi} compartment was not replenished appreciably by Pax7-nGFP^{Lo} cells (Figures 3Ia–3Id). These observations suggest that Pax7-nGFP^{Hi} cells are more upstream and that they give rise to Pax7-nGFP^{Lo} satellite cells.

Cells Performing TDSS Are Enriched in the Pax7^{Hi} Satellite Cell Subpopulation

To determine which subpopulation of satellite cells can perform TDSS in vivo, we employed a strategy similar to that indicated above but with regenerating muscle. The Tibialis anterior muscle of 6-week-old *Tg:Pax7-nGFP* mice was injured by intramuscular injection of the snake venom notexin (Gayraud-Morel et al., 2007; Figure 4A). Rapid degeneration and necrosis of myofibers occur, and satellite cells are concomitantly activated to generate myoblasts that will participate in muscle regeneration, usually taking about 3–4 weeks before homeostasis is achieved. BrdU was administered intraperitoneally from the second (D2) to the fifth (D5) day postinjury, and animals were sacrificed at different times after the last injection (Figure 4A). Consistent with the growth paradigm, LRCs were enriched in the Pax7-nGFP^{Hi} subpopulation at all times examined (e.g., after 11 weeks 12% in Pax7-nGFP^{Hi} versus 3.9% in Pax7-nGFP^{Lo} satellite cells; Figure 4B).

The higher frequency of LRCs observed in the Pax7-nGFP^{Hi} subpopulation might be a consequence of this subpopulation entering quiescence more rapidly than Pax7-nGFP^{Lo} cells. To investigate this possibility, satellite cells were isolated at time intervals after injury, and the mice were injected with BrdU prior to sacrifice. No difference was detected in the frequency of

(F) Quantification by immunofluorescence of LRCs. n = 300-400 cells; n = 3–8 mice per time point.
(G–J) Representative images of LRCs from total population at different time points: T0, 3.5, 7.5, and 11.5 weeks after the last BrdU (red) injection. Hoechst (blue).
(K) RT-qPCR analysis of relative gene expression in Pax7-nGFP^{Hi} and Pax7-nGFP^{Lo} subpopulations. n = 5–13 mice.
(L) Western blot showing the level of Pax7 protein in Pax7-nGFP^{Hi} and Pax7-nGFP^{Lo}. Tubulin as a normalizer.
(M) Flow cytometry showing that CD34 is upregulated in the Pax7-nGFP^{Hi} subpopulation.
Error bars represent ± SD. Scale bars, 10 μm (A–C) and 20 μm (G–J).

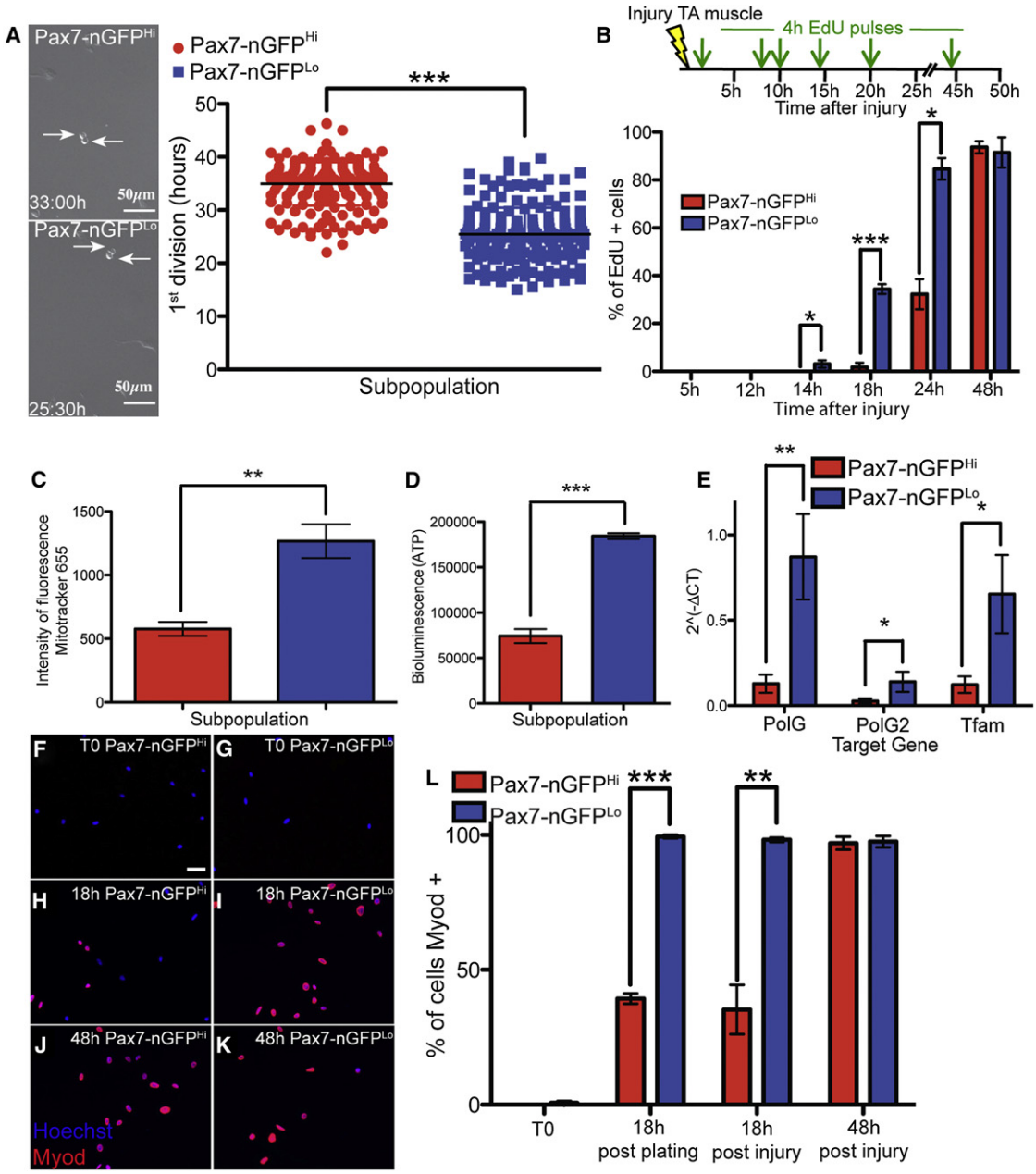

Figure 2. Pax7-nGFP^{Hi} Cells Display More Stem-like Markers, Lower Metabolic State, and Greater Lag before First Cell Division

(A) Video microscopy of Pax7-nGFP^{Hi} and Pax7-nGFP^{Lo} subpopulations. The first division was scored, and a cell was considered to have divided when cytokinesis was completed. Arrows indicate dividing cells. In low oxygen, mean times were 27 and 18 hr, respectively, and then every 7–8 hr for both.

(B) Percentage of EdU^{+} satellite cells in each fraction after injury. EdU was administered 4 hr before sacrifice.

(C) Active mitochondria were scored by adding MitoTracker, and intensity was measured in arbitrary units by flow cytometry (633 nm).

(D) Quantification of ATP in arbitrary units measured by bioluminescence (luminometer).

(E) RT-qPCR of mitochondrial replication genes to monitor mitochondrial activity.

(F–K) Immunostaining for Myod postinjury at T0, 18 hr, and 48 hr calculated from the time of isolation of satellite cells for in vitro and from the time of injury for in vivo. n = 300 cells; n = 4 mice.

(L) Histogram representing percentage of Myod+ cells in vitro (postplating) and in vivo (postinjury).

Error bars represent ± SD (SEM for E). Scale bars, 50 μm (A) and 20 μm (F–K).

BrdU^{+} cells in the two subpopulations, indicating that Pax7-nGFP^{Hi} cells do not exit the cell cycle preferentially in this case (Figure S1A).

We then investigated whether selective label retention in the Pax7-nGFP^{Hi} subpopulation might be a result of cosegregation of template DNA strands to one daughter cell during cell division.

To do so, EdU labeling was used to monitor TDSS (72 hr postinjury for 2 days), and BrdU was added to ensure that cells continued to divide during this period (during 18 hr chase of EdU; see Figures 4C and 4F). Notably, during this latter period (5–6 days postinjury), we determined that the cell-cycle period in vivo was comparable in both subpopulations (~8 hr; Figures S1B and S1C; Extended Experimental Procedures), thereby confirming results obtained by live video microscopy (Figure 2A). To detect TDSS empirically (Figure 4F), cells with EdU-labeled template DNA strands are considered as the starting population (T0). After one cell division (T1) and in the presence of BrdU, daughter cells are positive for both nucleotide analogs. TDSS can be observed empirically after two cell divisions (T2) wherein BrdU-positive daughter cells are either EdU positive or negative (biased segregation). Both daughters are positive for both labels during nonbiased DNA segregation.

Pax7-nGFP^{Hi} and Pax7-nGFP^{Lo} subpopulations were isolated by FACS and either fixed immediately after isolation (T1), or plated for 12 hr on a culture dish to allow cell-cycle progression and the second cell division (T2). The T1 analysis serves as a critical control because it showed that over 95% of the cells were strongly positive for both analogs in both subpopulations (Figures S1D and S1E); therefore, virtually all myogenic cells were actively dividing. As a separate control, to examine the minor fraction of BrdU-negative cells (<5%; Figure 4G), animals were pulsed with BrdU, and satellite cells were fractionated into different subpopulations based on GFP intensity. All subpopulations incorporated BrdU with no apparent bias, indicating that the minor BrdU-negative fraction is due to a general inefficiency in BrdU uptake among all GFP-expressing satellite cells (data not shown).

After two cell divisions (T2) in the absence of EdU, similar numbers of cells were positive for both analogs in the Pax7-nGFP^{Lo} subpopulation, with the majority being positive for BrdU and EdU (Figures 4E and 4G). Significantly, however, 40% of Pax7-nGFP^{Hi} cells were EdU negative, whereas all were BrdU positive, indicating that they continued to proliferate during the chase period (Figures 4D and 4G). To confirm these observations, these experiments were repeated, and both subpopulations were analyzed by flow cytometry at T1 and T2. After one cell division during the chase at T1, ~96% of the cells were positive for both BrdU and EdU in both subpopulations (Figures 4H and 4J). After a second cell division at T2, ~56% were EdU^{+}/BrdU^{+}, and ~44% were EdU^{-}/BrdU^{+} in the Pax7-nGFP^{Hi} fraction, whereas ~92% were EdU^{+}/BrdU^{+} in the Pax7-nGFP^{Lo} fraction (Figures 4I and 4K). From these results, we propose that 87% of the Pax7-nGFP^{Hi} fraction performs TDSS (i.e., 43.5% negative and 43.5% positive daughter cells). In addition, extending the gating conditions to include more intermediate Pax7-nGFP+ cells resulted in a drop in the frequency of TDSS, suggesting that TDSS is restricted to the Pax7-nGFP^{Hi} cells (data not shown). After biased DNA segregation, it is expected that the EdU intensity would remain the same in the Pax7-nGFP^{Hi} subpopulation due to inheritance of all EdU-labeled DNA strands in only one daughter cell, whereas random distribution of EdU-labeled strands in the Pax7-nGFP^{Lo} subpopulation would result in approximately half the signal intensity in daughter cells at the population level. Expectedly, both subpopulations displayed the same intensity for EdU staining at T1 (geometric mean: 660 and 669, respectively). Notably, at T2 the Pax7-nGFP^{Hi} subpopulation contained cells with an EdU intensity similar to that at T1 (mean: 590), and cells with no signal (mean: 10), as expected if this subpopulation performed TDSS. By contrast, the population mean intensity for Pax7-nGFP^{Lo} cells dropped to half the intensity of that observed at T1 (mean: 350), as expected for random segregation of EdU-labeled chromatids. Identical results were obtained when these experiments were repeated and when the second division took place in vivo (data not shown). Therefore, the Pax7-nGFP^{Hi} subpopulation is enriched in cells that perform template DNA strand cosegregation, whereas Pax7-nGFP^{Lo} cells segregate their chromatids randomly.

Fate of Muscle Stem Cells Cosegregating Template DNA Strands

During lineage commitment, *Pax7* expression is downregulated as differentiation proceeds (Zammit et al., 2004). Given that TDSS is restricted to the Pax7-nGFP^{Hi} subpopulation, we investigated the fate of the resulting daughter cells. To do this, activated satellite cells were isolated 5 days postinjury according to GFP signal intensity (Figure 5A). In keeping with our observations with quiescent satellite cells, transcript analysis and FACS profiling showed higher *Pax7* and CD34 expression in Pax7-nGFP^{Hi} cycling cells, and lower levels of commitment genes such as Sca1 (Figures 5B and S2A–S2E). Accordingly, myogenic commitment markers Sca1, Desmin, and TroponinT were expressed at higher levels in the Pax7-nGFP^{Lo} cells (Figure 5B). Additionally, 33.1% of Pax7-nGFP^{Lo} cells were positive for the differentiation protein Myogenin compared to 4.5% in the Pax7-nGFP^{Hi} fraction (Figures S2A–S2C). Taken together, these observations indicate that the Pax7-nGFP^{Hi} subpopulation of cycling myogenic cells that cosegregate template DNA strands expresses higher levels of stem-like markers, and lower levels of markers associated with myogenic commitment.

If differential gene regulation in daughter cells was a consequence of TDSS, cells retaining old template DNA strands in the Pax7-nGFP^{Hi} subpopulation should be more stem like, whereas their sister cell inheriting nascent DNA strands should be more committed. To test for this premise, we developed a protocol to isolate EdU-positive and EdU-negative cells from the Pax7-nGFP^{Hi} subpopulation two cell divisions after EdU administration (T2), immediately after biased DNA segregation and mitosis (see Figure 4F). EdU injections were performed 4 days postinjury of the Tibialis anterior muscle, and this was followed by a chase for one cell division in vivo (T1) in the absence of the thymidine analog. Satellite cells were fractionated into Pax7-nGFP^{Hi} and Pax7-nGFP^{Lo} by FACS, then plated for 12 hr to complete the second division (T2). In this paradigm, template DNA retaining and excluding cells would be EdU positive or negative, respectively. The cells from each initial fraction (Pax7-nGFP^{Hi} and Pax7-nGFP^{Lo}) were then fixed, stained for EdU, and subjected to a second round of FACS (Figure 5C). Strikingly, RT-qPCR analysis showed that Pax7-nGFP^{Hi} cells that were EdU-positive cells expressed significantly higher levels of endogenous *Pax7* and *nGFP* transcripts, and lower levels of the differentiation markers Myogenin and Troponin T compared to EdU-negative cells (Figure 5D).

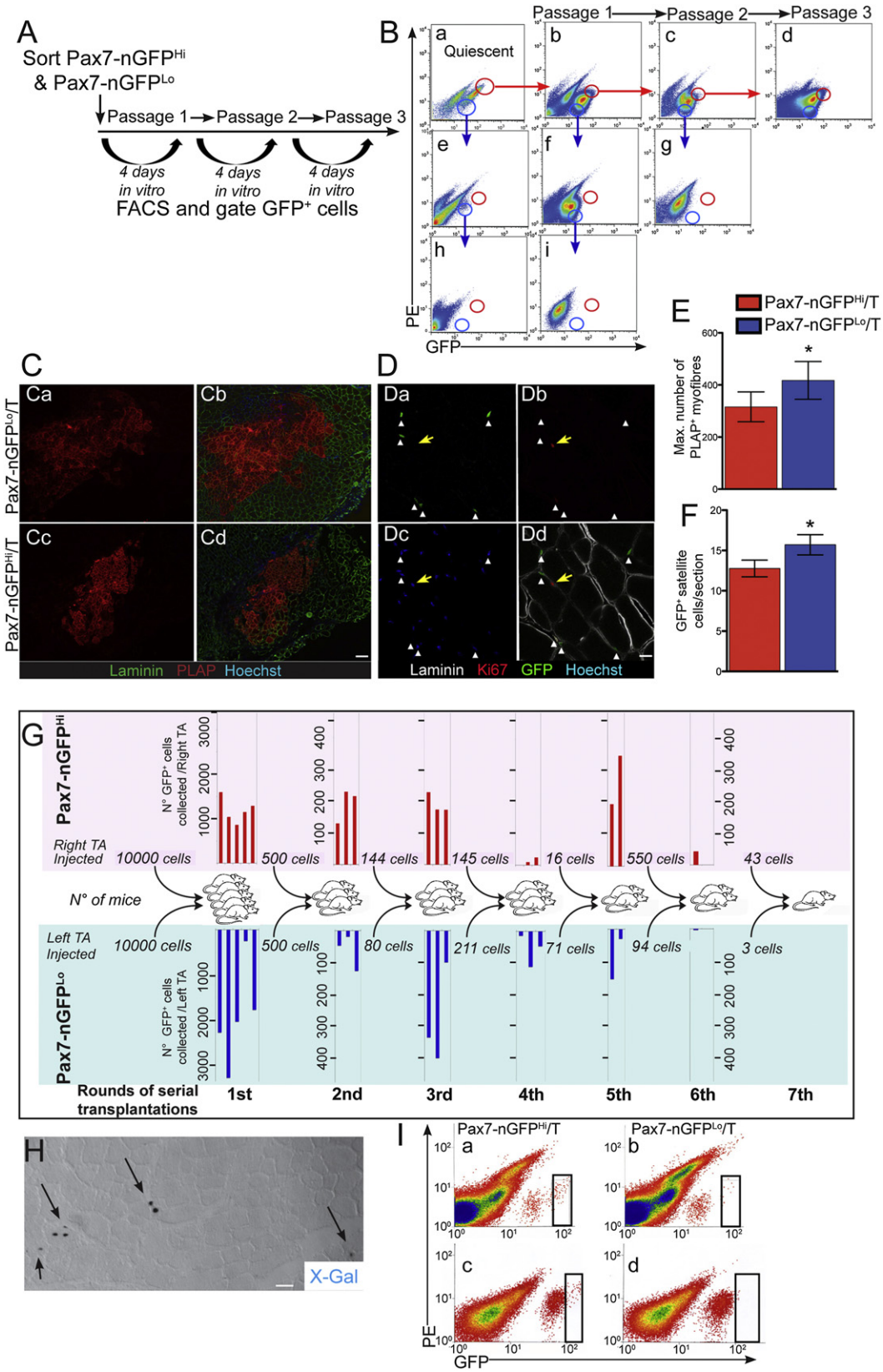
A
Sort Pax7-nGFPHi
& Pax7-nGFPLo
Passage 1
Passage 2
Passage 3
4 days in vitro
4 days in vitro
4 days in vitro
FACS and gate GFP+ cells
B
Passage 1
Passage 2
Passage 3
a Quiescent
b
c
d
e
f
g
h
i
PE
GFP
C
Ca
Cb
Cc
Cd
Pax7-nGFPLo/T
Pax7-nGFPHi/T
Laminin PLAP Hoechst
D
Da
Db
Dc
Dd
Laminin Ki67 GFP Hoechst
E
Pax7-nGFPHi/T
Pax7-nGFPLo/T
Max. number of PLAP+ myofibres
F
GFP+ satellite cells/section
G
Pax7-nGFPHi
N° GFP+ cells collected /Right TA
Right TA Injected
10000 cells
500 cells
144 cells
145 cells
16 cells
550 cells
43 cells
N° of mice
Left TA Injected
10000 cells
500 cells
80 cells
211 cells
71 cells
94 cells
3 cells
Pax7-nGFPLo
N° GFP+ cells collected /Left TA
Rounds of serial transplantations
1st
2nd
3rd
4th
5th
6th
7th
H
X-Gal
I
Pax7-nGFPHi/T
Pax7-nGFPLo/T
a
b
c
d
PE
GFP

To determine whether these cells were truly committed, and not simply transcriptionally primed, from the same experiment an aliquot of cells from both subpopulations was either fixed immediately after one cell division (T1), or plated and fixed after the second cell division (T2). A critical control was the demonstration that all of the cells were EdU$^+$ at T1 in the Pax7-nGFP^{Hi} fraction (Figures S2F and S2G). Notably, 41% of Pax7-nGFP^{Hi} cells were EdU negative after the second cell division (T2, Figures 5F and 5G; 82% of Pax7-nGFP^{Hi} performs TDSS; i.e., 41%-negative and 41%-positive daughter cells), consistent with experiments reported above. At T2 only the EdU-negative cells (inheriting nascent DNA strands) expressed Myogenin protein (42%; Figures 5E and 5F). Conversely, none of the EdU$^+$ cells (retaining template DNA strands) expressed this differentiation marker. In contrast, in the Pax7-nGFP^{Lo} subpopulation all of the cells were positive for EdU at T1 as well as T2, as observed above (Figures 5E and 5G). Notably, 32% of the cells were positive for Myogenin at T1 and 94% at T2 (Figures 5E and 5G), in support of the findings above that this subpopulation is more committed to differentiation. Similar results were obtained with the differentiation marker TroponinT (Figures S2H–S2J). Taken together, these results show that within the Pax7-nGFP^{Hi} subpopulation, cells that retain template DNA strands adopt a more stem-like phenotype, whereas those that inherit nascent DNA strands differentiate. In contrast, the Pax7-nGFP^{Lo} cells perform random DNA segregation and are myogenically committed.

Template DNA Strand Cosegregation during Cell Division Engages All Chromatids

Previous studies reported that some but not all chromatids are involved in nonrandom segregation of DNA strands (Armakolas and Klar, 2006; Falconer et al., 2010). In our previous studies and those reported here, immunofluorescence staining for nucleotide analogs suggested that TDSS in satellite cells involves all chromatids because the analog-negative cells showed little to no label retention, although single-chromosome resolution was lacking. To determine the number of chromosomes that participate in TDSS, CO-FISH (Bailey et al., 1996; Falconer et al., 2010) was performed. Here, BrdU-containing strands are eliminated selectively by treatment of cells with Hoechst, UV light, and exonuclease III. Direct visualization of chromatids on metaphase spreads, combined with hybridization with specific leading and lagging strand telomeric probes, permits the enumeration of BrdU-containing chromosomes. Mice were injected repeatedly with BrdU to saturate newly formed DNA strands 3 days postinjury of the Tibialis anterior muscle (Figure 6A). Pax7-nGFP^{Hi} and Pax7-nGFP^{Lo} cells were then isolated either after one cell division in vivo and a second in vitro, or both divisions in vivo, without analog, and telomere-specific probes were used to detect individual DNA strands on metaphase cells (Figure 6B and data not shown, respectively). Chromosomes having one BrdU$^+$ DNA strand exhibit six discrete signals in a head to tail arrangement: three belonging to telomeres located on the leading strands, and three to the lagging strands. BrdU-negative chromosomes exhibit eight signals: four belonging to telomeres located on the leading strands, and four to the lagging strands (Figure 6B). Each chromosome of each metaphase was analyzed.

As a control, and immediately after the last BrdU injections (T0), all chromosomes from virtually all metaphases in the subpopulations contained BrdU-saturated neosynthesized DNA strands (Figures S3A–S3D). This critical control shows that all of the cells in both subpopulations were in the cell cycle, and that they incorporated BrdU. During random DNA segregation a three dot/four dot pattern should be observed in every cell. This was indeed the case for the Pax7-nGFP^{Lo} subpopulation (Figures 6C, 6F, and S4). Strikingly, however, individual cells with distinct patterns of either three dots, or four dots, were

Figure 3. Engraftment Potential of Subpopulations of Satellite Cells

(A) Scheme of serial plating of both subpopulations.

(Ba–Bi) FACS profiles of serial passages of both subpopulations. Red circles indicate Pax7-nGFP^{Hi}; blue circles show Pax7-nGFP^{Lo}. After each passage, each subpopulation was replated independently, and cultures were subjected again to FACS analysis.

(Ca–Cd) Cryodamaged *Rag2*$^{-/-}$:$\gamma C^{-/-}$ mice were transplanted with 10^4 freshly sorted *Tg:Pax7-nGFP*^{Hi}/T and *Tg:Pax7-nGFP*^{Lo}/T satellite cells and analyzed 4 weeks later. Representative images of donor-derived PLAP$^+$ myofibers are indicated.

(Da–Dd) Representative image of a TA muscle 4 weeks postinjury. White arrowheads show GFP$^+$ satellite cells, yellow arrows indicate a Ki67-positive interstitial cell, and white illustrates Laminin.

(E) Average of maximum number of PLAP$^+$ myofibers generated from *Tg:Pax7-nGFP*^{Hi}/T and *Tg:Pax7-nGFP*^{Lo}/T cells 4 weeks after engraftment (n = 7 mice/condition; p = 0.02).

(F) Engrafted satellite cells scored as GFP$^+$/PLAP$^+$ 4 weeks after transplantation represented as average number of GFP$^+$ cells for all sections (*Tg:Pax7-nGFP*^{Hi}/T, n = 7 mice, n = 90 sections; *Tg:Pax7-nGFP*^{Lo}/T, n = 7 mice, n = 90 sections; p = 0.02).

(G) Serial transplantations of *Tg:Pax7-nGFP*^{Hi}/T and *Tg:Pax7-nGFP*^{Lo}/T satellite cell subpopulations in each preinjured TA of *Rag2*$^{-/-}\gamma C^{-/-}$ mice. GFP$^+$ cells were isolated by FACS 3 weeks posttransplantation. For subsequent transplantations all GFP$^+$ cells isolated from *Tg:Pax7-nGFP*^{Hi}/T or *Tg:Pax7-nGFP*^{Lo}/T fractions were pooled independently and divided equally among animals. Illustration represents seven rounds of comparative transplantations with each subpopulation. The last round did not yield GFP$^+$ satellite cells.

(H) X-gal staining of a section of injured and engrafted Tibialis anterior muscle 4 weeks postinjury. Blue nuclei show that grafted cells contribute to muscle regeneration. Arrows indicate X-gal positive myofibers.

(Ia–Id) FACS profile of engrafted GFP$^+$ satellite cells (Pax7-nGFP^{Hi}/T and Pax7-nGFP^{Lo}/T) after isolation. In two independent experiments (Ia and Ib, Ic and Id, and data not shown), only Pax7-nGFP^{Hi} cells gave GFP^{Hi} cells (vertical rectangle gate on right); Pax7-nGFP^{Lo}/T cells did not yield significant numbers of GFP^{Hi} cells; FACS profiles represent first passage from the two independent experiments. Gating was done on GFP intensity during isolation of top or bottom 10% of the number of cells in the GFP$^+$ population. The high fraction was often distinct from the main population on the FACS profile. There was a total of 81 GFP^{Hi}/476 GFP$^+$ cells (Ia), 10 GFP^{Hi}/512 GFP$^+$ cells (Ib), 110 GFP^{Hi}/1,597 GFP$^+$ cells (Ic), and 18 GFP^{Hi}/2,288 GFP$^+$ cells (Id).

For each sorting (B and I), gates were adjusted similarly to isolate numerical 10% high or low GFP$^+$ fractions. Error bars represent ±SEM. Scale bars, 50 μm (C and H) and 20 μm (D).

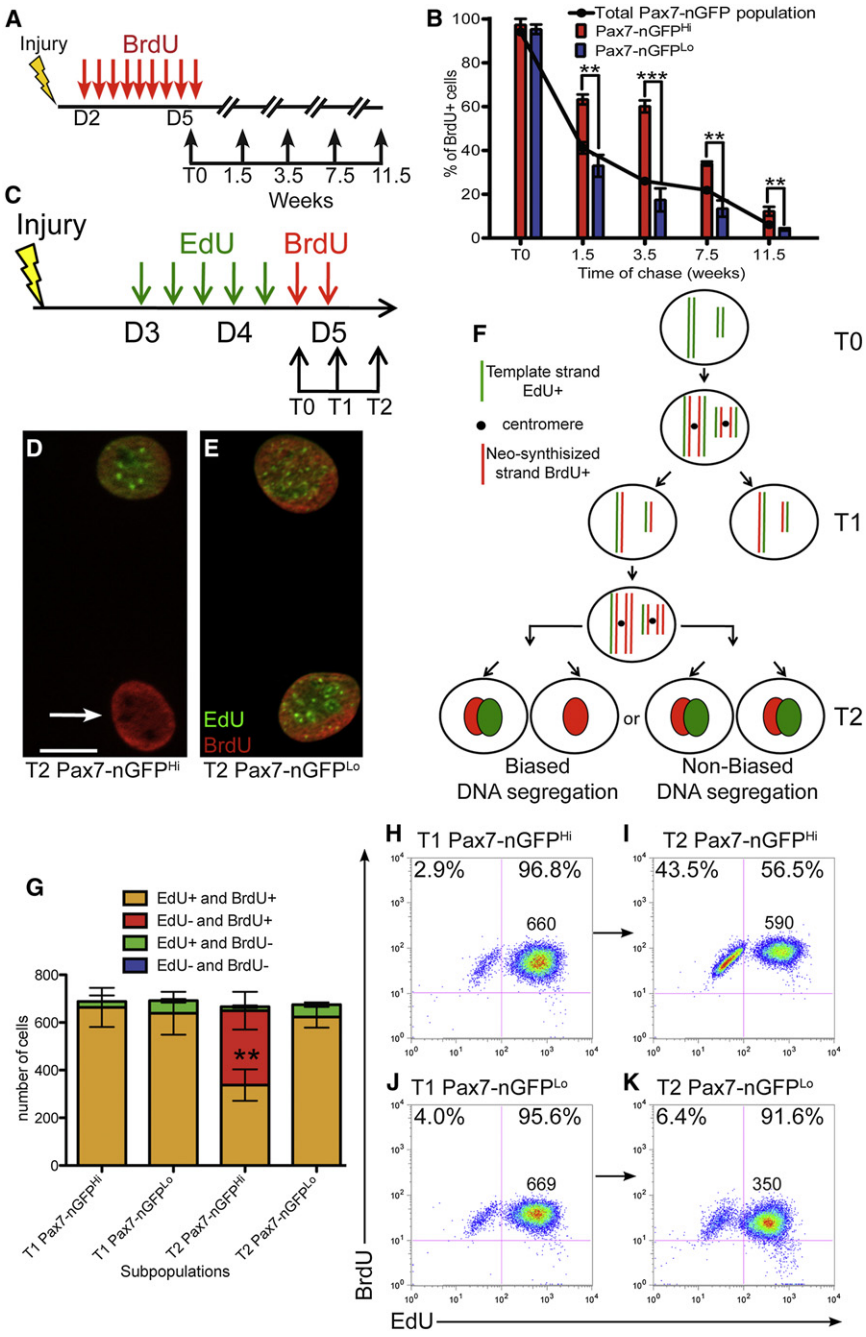

Figure 4. Pax7-nGFP^{Hi}, but Not Pax7-nGFP^{Lo}, Muscle Satellite Cells Perform TDSS

(A) Scheme of muscle injury and timing of BrdU injections in *Tg:Pax7-nGFP* mice to generate LRCs.

(B) Quantification by immunofluorescence of LRCs. Histogram represents percentage of cells retaining BrdU in each subpopulation; n = 4 mice, ≥300 cells each.

(C) Scheme of timing of EdU and BrdU injections (7–8 hr apart) to monitor TDSS.

(D) Representative image of T2 Pax7-nGFP^{Hi} cells. Arrow indicates BrdU^{+} (red) cell that has excluded EdU (green).

(E) Representative image of T2 Pax7-nGFP^{Lo} cells.

(F) Scheme of biased (left) and nonbiased (right) segregation patterns.

(G) Histogram representing the number of cells retaining EdU and BrdU in each subpopulation at time of isolation (T1, one cell division during chase; and T2, after second cell division); n = 4 mice, ≥300 cells at T1, ≥500 at T2.

(H–K) Flow cytometry analysis of both subpopulations for EdU and BrdU intensity: (H) T1 Pax7-nGFP^{Hi} ; (I) T2 Pax7-nGFP^{Hi}; (J) T1 Pax7-nGFP^{Lo}; and (K) T2 Pax7-nGFP^{Lo}. Numbers in corners represent percentage (%) of cells; geometric mean intensities of EdU labeling are indicated. On profile, red color indicates high cell density, and blue color shows low cell density; n = 4 mice, ≥3,000 cells each condition.

Error bars represent ±SD. Scale bar, 10 μm (D and E). See also Figure S1.

observed only in the Pax7-nGFP^{Hi} subpopulation, as predicted for cells containing either hemi-labeled BrdU DNA strands, or cells with no BrdU-labeled strands, respectively (85% n = 150 cells, three independent experiments; Figures 6C–6E and S5–S7). Some cells with mixed patterns were observed in this subpopulation, consistent with our findings using EdU and BrdU. Therefore, these results show with single-chromosome resolution that the majority of the cells in the Pax7-nGFP^{Hi} subpopulation performs TDSS in vivo, whereas random DNA segregation occurs in the Pax7-nGFP^{Lo} subpopulation.

DISCUSSION

Recent investigations have suggested that skeletal muscle satellite cells are heterogeneous, harboring stem-like and more committed cells; however, the lack of readouts has hampered more detailed analyses. Here, we identify prospectively a subpopulation of proliferating satellite cells, corresponding to high *Pax7* expression with a low metabolic state, the majority of which reproducibly performs TDSS. Importantly, we show that all template DNA strands segregate to the daughter cell acquiring a stem cell fate, whereas daughter cells that inherit nascent DNA strands differentiate. The rapid upregulation of multiple stem and differentiation markers in the respective daughter cells provides compelling evidence that template DNA strand cosegregation is associated with, and perhaps a critical element in, regulating this cell fate decision.

Interestingly, we show also that in the quiescent state a subpopulation of cells expressing higher levels of *Pax7* has a low metabolic state, is transcriptionally less primed for myogenic commitment, and takes longer to execute the first mitosis after

being stimulated to enter the cell cycle, yet subsequently it adopts a cell-cycle time equivalent to the remaining population. We refer to this reversible cell state as dormant. Dormant hematopoietic stem cells (HSCs) have been reported to be BrdU label retaining, and divide about five times per lifetime in the mouse (Wilson et al., 2008). Further characterization of those cells should determine if the characteristics reported here regarding cell-cycle entry time after activation and metabolic status are shared features of dormant muscle and HSCs.

Serial transplantation studies to assess the long-term regenerative potential of stem cells have been reported routinely for HSCs and skin stem cells, but not extensively for other tissue-specific stem cells. In our study, serial transplantation experiments were performed for up to 7 rounds with as little as 16 cells, thereby providing evidence that satellite cells are indeed long-lasting stem cells, and that extensive symmetric divisions occur for at least a subpopulation of transplanted cells. These findings complement our satellite cell ablation studies, which resulted in failed regeneration, and rescue with transplanted satellite cells (Sambasivan et al., 2011).Furthermore, only $Pax7^{Hi}$-expressing cells replenished the $Pax7^{Hi}$ GFP^{+} fraction, providing compelling evidence that cells performing TDSS are at the top of the stem cell hierarchy characterized by high levels of *Pax7* expression. How asymmetric DNA segregation relates to asymmetric versus symmetric cell divisions over extended periods is not clear. A central premise of the "immortal" DNA strand hypothesis (Cairns, 1975) presumes the occurrence of obligate, consecutive asymmetric DNA segregation, with no intervening symmetric cell divisions to reduce the mutation load due to accumulated DNA replication errors. Whether this occurs, or if epigenetic regulation is the primary mechanism driving TDSS to regulate daughter cell fates through chromatin modifications, for example, are notions that remain to be tested. Whichever the case, symmetric cell divisions might be tolerated occasionally. Moreover, we cannot exclude the possibility that all muscle stem cells might, under certain conditions, perform biased DNA segregation.

In the present report, we employed several strategies to demonstrate that TDSS occurs in a subpopulation of satellite cells with more stem-like properties. In addition, using CO-FISH and single-chromatid resolution, we provide the first evidence for asymmetric DNA segregation involving all chromosomes. Notably, the ability to prospectively isolate these cells provides a powerful tool for more detailed characterization of this population. Strikingly, the asymmetric segregation of DNA in the $Pax7^{Hi}$ fraction is associated with an immediate cell fate change. Several markers were used, including Sca1, which is associated with committed cells (Mitchell et al., 2005). This is in contrast to a previous study reporting that template DNA strands segregate with Sca1 (Conboy et al., 2007). The different results obtained with this marker warrant further investigation. Another issue that has not been addressed is the role of halogenated nucleotides, which have been used almost exclusively to monitor DNA segregation patterns (Cortés et al., 2003; Tajbakhsh and Gonzalez, 2009).

In conclusion, our findings provide the first evidence for template DNA strand cosegregation with single-chromatid resolution, and they identify a subpopulation of muscle stem cells with a low metabolic state that reproducibly retains template DNA strands. The ability to isolate these cells prospectively will allow more detailed studies of this phenomenon in relation to cellular asymmetry, the physiological status of the cells, and the epigenetic regulation of stem cell fate.

EXPERIMENTAL PROCEDURES

Mice and Injections of Thymidine Analogs

Tg:Pax7-nGFP mice were described previously (Sambasivan et al., 2009). Thymidine analogs (Sigma-Aldrich, St. Louis) were dissolved in 0.9% saline (GIBCO, Paisley, UK) and stored at 10 mg/ml. For pulse-chase experiments during postnatal growth, P3 mice received single doses of BrdU at 3 μg/g intraperitoneally, twice a day, for 6 consecutive days followed by 4–11 weeks of chase. For the pulse-chase labeling after notexin injury, transgenic mice (6–10 weeks old) received 50 μg/g BrdU five times 8 hr apart followed by 4–11 weeks of chase. To detect biased segregation of chromosomes, mice were injected intraperitoneally 3 days postinjury with EdU (Invitrogen, Carlsbad, CA, USA; #C10339) five times, 200 μg/injection 8 hr apart followed by the injection of BrdU (twice 8 hr apart) 8 hr after EdU. Animals were handled as per European Community guidelines.

Satellite Cell Culture and FACS

Satellite cells have been cultured in 1:1 DMEM:MCDB containing 20% serum FBS and ITS (1×, Insulin Transferrin Selenium; GIBCO). Medium was filtered through 22 μm. Cells were plated on Matrigel (BD Biosciences; catalog #354234) and kept in an incubator (37°C, 6.5% CO_2, 3% O_2). Cells were prepared for FACS analysis using a MoFlo (Beckman). All analyses and quantitations were performed using Summit v4.3 software from DakoCytomation and FloJo software. Cells were labeled with Propidium Iodide 10 μg/ml (Sigma-Aldrich) to exclude dead cells and displayed using the PE (Phycoerythrin, Red) channel on the FACS profile. Dissection was done essentially as described (Gayraud-Morel et al., 2007) with a scalpel by removing the tissue from the bone in cold DMEM. Muscles were then chopped with small scissors and put in a 50 ml Falcon tube with collagenase 0.1% and trypsin 0.25% at 37°C with gentle agitation. The supernatant was collected in serum on ice after 20 min, and the collagenase/trypsin solution was added to continue the digestion until the muscle was completely digested; it was filtered through 40 μm filter.

Muscle Injury and Serial Satellite Cell Transplantations

Immunocompromised $Rag2^{-/-}{:}\gamma C^{-/-}$ mice were injured by freeze injury 2 days prior to cell engraftment. Briefly, mice were anesthetized with 0.5% Imalgene/2% Rompun. The TA muscle was frozen with three consecutive cycles of freezing-thawing by applying a liquid nitrogen-cooled metallic rod. The skin was sutured, and mice were kept on a warm plate until recovery. Satellite cells collected by FACS were centrifuged 15 min in an Eppendorf centrifuge at 550× *g*. The supernatant was carefully eliminated, and the pellet was resuspended in a minimal volume to inject 5–10 μl of cell suspension per TA. Cell suspensions were enumerated using a Malassez counting chamber to adjust the concentration of cells injected in preinjured TA with a 10 μl Hamilton syringe. Three weeks after transplantation, mice were sacrificed by cervical dislocation, and the tissue was analyzed. For quantifications, the entire TA muscle was sectioned, and at least four different, evenly spaced levels were stained and used for $PLAP^{+}$ myofiber and GFP^{+} satellite cell enumerations after immunostainings. Figures display average values of all animals tested ±SEM.

Gene Expression Analysis

Extraction and preparation of RNA for RT-qPCR were done as described (Jory et al., 2009). Cells were sorted directly in RLT lysis buffer (Invitrogen) containing β-mercaptoethanol, and RNA was purified using QIAGEN RNAeasy Micro purification kit. cDNA was generated by random-primed reverse transcription using the SuperScript II reverse transcriptase (Invitrogen). The cDNAs were then analyzed by real-time PCR (see Table S1 for primers) using Power SYBR Green Universal Mix or TaqMan Universal Master Mix and an ABI Prism 7700 (PerkinElmer Applied Biosystems) and a StepOnePlus

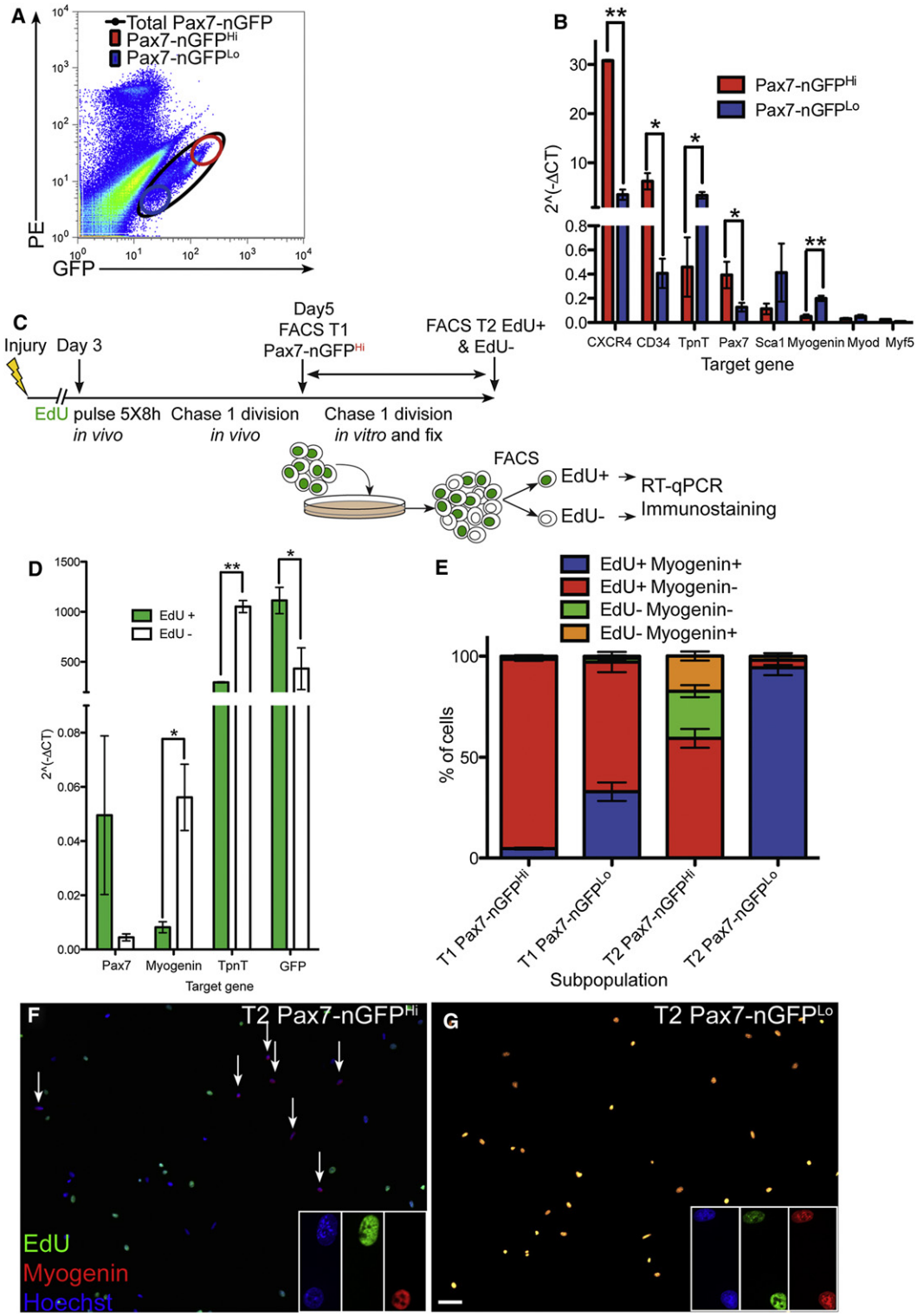

Figure 5. Muscle Stem Cells Inheriting Template DNA Strands Retain Stem Cell Properties

(A) FACS profile of GFP^{+} satellite cells from injured *Tg:Pax7-nGFP* TA muscle D5 postinjury. Gating for Pax7-nGFP^{Hi} and Pax7-nGFP^{Lo} is indicated.

(B) RT-qPCR of stem and differentiation markers in Pax7-nGFP^{Hi} and Pax7-nGFP^{Lo} cells isolated as indicated in (A); n = 5 mice, 20,000 cells/condition.

(C) Scheme for isolation of template DNA strand retaining (EdU^{+}) and excluding (EdU^{-}) daughter cells from Pax7-nGFP^{Hi} subpopulation examined at T1 and T2. As a control, T1 cells in Pax7-nGFP^{Hi} and Pax7-nGFP^{Lo} subpopulations were isolated by FACS and analyzed.

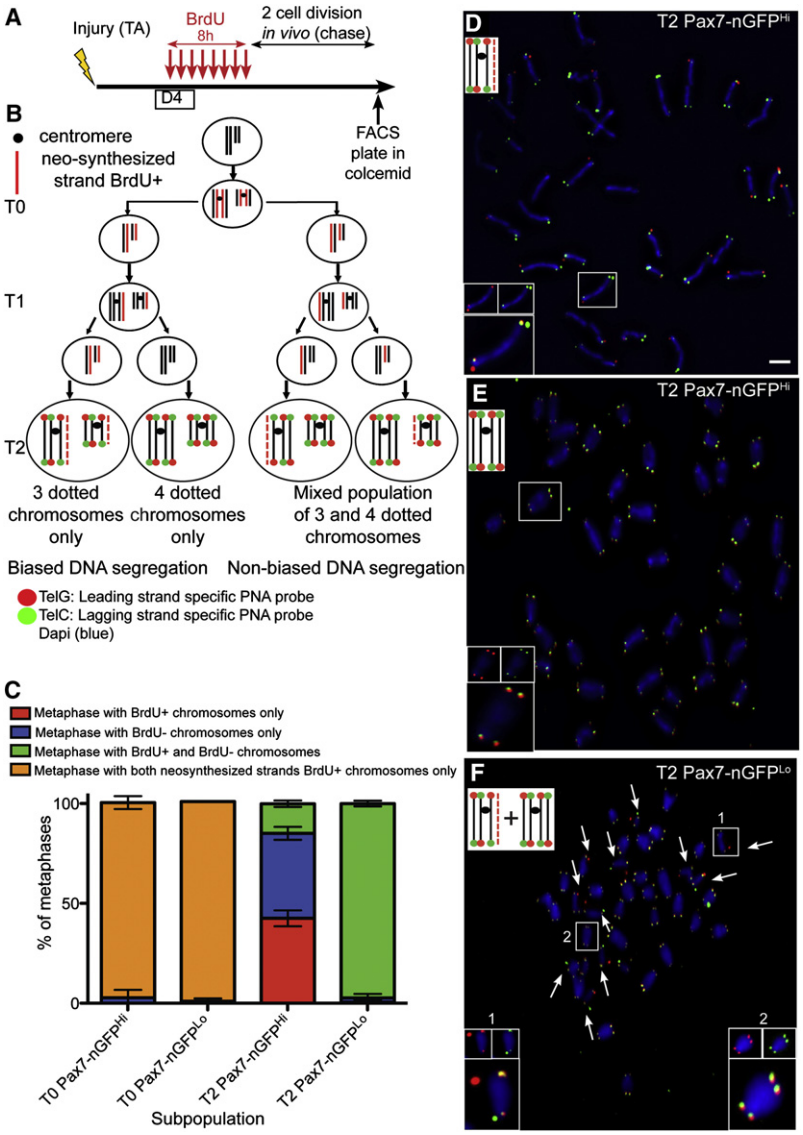

Figure 6. Identification of Sister Chromatids and Evidence for Template DNA Strand Cosegregation in Pax7-nGFP^{Hi} Muscle Stem Cells

(A) Scheme of BrdU injections and isolation of satellite cells.

(B) Scheme of TDSS and nonbiased DNA segregation with leading and lagging strands represented, and segregation patterns of sister chromatids that are BrdU^{+} (three dots) or BrdU^{-} (four dots).

(C) Percentage of metaphases displaying the different observed patterns of chromatid segregation with PNA probes. Quantifications were done for both subpopulations at the time of isolation without chase (T0) and at T2 (after two cell divisions); n = 150 cells each; three independent experiments. All DNA strands show an exclusive staining with PNA probes specific for either leading or lagging strands.

(D) Metaphase analysis after the second cell division (T2) of Pax7-nGFP^{Hi} cell-containing BrdU-positive chromosomes only. Insets represent high magnification of chromosome (boxed). Arrows indicate BrdU^{+} chromosomes.

(E) Metaphase of T2 Pax7-nGFP^{Hi} cell-containing BrdU-negative chromosomes only. Insets represent high magnification of chromosome (boxed).

(F) Metaphase of T2 Pax7-nGFP^{Lo} cell-containing BrdU-positive and negative chromosomes. Insets represent high magnification of chromosome (boxed).

Error bars represent ± SD. Scale bars, 5 μm (D–F). See also Figures S3–S7.

(Applied Biosystems). TBP reference transcript levels were used for the normalization of each target within each sample (= ΔCT).

Immunohistochemistry

Immunostaining was performed on fixed cells (4% PFA in cold PBS), permeabilized with 0.5% Triton X-100 5 min, washed, and blocked with 10% BSA. For the BrdU immunostaining, cells were unmasked with 2 N HCl 20 min at room temperature and neutralized with 0.1 M sodium tetraborate. For EdU staining, click-it reaction was used according to the manufacturer's instructions (Invitrogen). Cells were incubated with primary antibodies overnight at 4°C (see Table S2). Cells were washed with PBS and 0.1% BSA and then incubated 2 hr with Alexa-conjugated secondary antibodies 1/250 and Hoechst. Cells were then analyzed using a confocal Leica or Zeiss Apotome. For the assessment of cell fate after TDSS, instead of lysis buffer, the cells were collected in 2% serum, and both subpopulations were either spun on polyD-lysine and fixed immediately (T1) or plated overnight for them to complete their second division (T2).

Live Imaging

Cells isolated by FACS were plated overnight on a 24-well glass bottom plate (P24G-0-10-F; MatTek) precoated with Matrigel in the incubator in a drop of pre-equilibrated medium (1:1 DMEM GlutaMAX: MCDB [Sigma-Aldrich], 20% FCS [GIBCO; 22477K]). The plate was then incubated at 37°C, 5% CO_2, and 3% O_2 (Zeiss, Pecon). A Zeiss Observer.Z1 connected with a LCI PlnN 10×/0.8 W DICII objective and AxioCam camera piloted with AxioVision was used. Cells were filmed for up to 1 week, and images were taken every 20 min with Brightfield and DICII filters and MozaiX 3X3 (Zeiss). The raw data were transformed and presented as a video.

CO-FISH

CO-FISH metaphase chromosomes (Bailey et al., 2004) were prepared from female *Tg:Pax7-nGFP* mice injected with BrdU at 150 μg/g every hour for 8 hr. Subpopulations were sorted by FACS either immediately after the last BrdU injection (T0 control) or after an overnight chase, then plated with colcemid at 0.2 μg/ml 90 min before collection. After hypotonic treatment in 0.03 M sodium citrate for 25 min at 37°C, cells were fixed in cold 3:1 methanol acetic acid, and metaphases were spread on prewashed 45% acetic acid slide. For CO-FISH, chromosomes were treated with RNase A and pepsin, and slides were incubated in Hoechst 33258 and irradiated with UV light at 5.4 J/cm^{-2}. Nicked DNA was removed after digestion with exonuclease III, and remaining

(D) RT-qPCR after EdU staining and reisolation of cells by FACS; n = 45 independent experiments, 2 mice pooled each, ≥30,000 cells each.

(E) Quantification of cells by immunostaining for EdU and Myogenin in both subpopulations at T1 and T2; n = 4 mice, ≥300 cells each condition.

(F and G) Representative images of EdU (green) and Myogenin (red) immunostainings at T2 in Pax7-nGFP^{Hi} (F) and Pax7-nGFP^{Lo} (G) subpopulations. Insets in (F) show EdU-negative/Myogenin-positive cell (arrows) and EdU-positive/Myogenin-negative cell. Insets in (G) show cells double positive for these markers.

Error bars represent ± SEM (SD for E). Scale bars, 20 μm (F and G). See also Figure S2.

DNA strands were hybridized to directly labeled fluorescent PNA probes specific for C- and G-rich telomere repeats (TelC-FAM FITC-OO-$(CCCTAA)_3$; TelG-Cy3 Cy3-OO-$(TTAGGG)_3$; Panagene). Pictures were acquired at 100×, and signals were treated with Volocity.

Statistics

Statistical analysis was performed with GraphPad Prism software using appropriate tests and a minimum of 95% confidence interval for significance; p values indicated on figures are < 0.05 (*), < 0.01(**), and < 0.001 (***). Figures display average values of all animals tested ± SD or ± SEM for RT-qPCR, or as indicated.

SUPPLEMENTAL INFORMATION

Supplemental Information includes Extended Experimental Procedures, seven figures, two tables, and three movies and can be found with this article online at doi:10.1016/j.cell.2011.11.049.

ACKNOWLEDGMENTS

For cytometry we thank M. Nguyen, P.-H. Commere, N. Aulner (PFC, Institut Pasteur, Paris), A. Henry (IMRB, UFR de Medecine, Créteil), and funding by the Conseil de la Region Ile-de-France (SESAME 2007, Imagole; given to S. Shorte). We thank also members of the lab for critical comments. M.A.B. is funded by grants from the MICINN, the European Union, the European Research Council (ERC), The Lilly Foundation, and the Korber European Research Award. S.T. acknowledges support from the Institut Pasteur, Association Recherche contre le Cancer, Association Française contre le Myopathies, Centre national de la recherche scientifique, Agence Nationale de la Recherche (ANR-06-BLAN-0039), EU Framework 7 projects EuroSysStem, Optistem, and the Fondation pour la Recherche Medicale.

Received: May 24, 2011
Revised: October 20, 2011
Accepted: November 3, 2011
Published: January 19, 2012

REFERENCES

Armakolas, A., and Klar, A.J. (2006). Cell type regulates selective segregation of mouse chromosome 7 DNA strands in mitosis. Science *311*, 1146–1149.

Bailey, S.M., Goodwin, E.H., Meyne, J., and Cornforth, M.N. (1996). CO-FISH reveals inversions associated with isochromosome formation. Mutagenesis *11*, 139–144.

Bailey, S.M., Brenneman, M.A., and Goodwin, E.H. (2004). Frequent recombination in telomeric DNA may extend the proliferative life of telomerase-negative cells. Nucleic Acids Res. *32*, 3743–3751.

Beauchamp, J.R., Morgan, J.E., Pagel, C.N., and Partridge, T.A. (1999). Dynamics of myoblast transplantation reveal a discrete minority of precursors with stem cell-like properties as the myogenic source. J. Cell Biol. *144*, 1113–1122.

Beauchamp, J.R., Heslop, L., Yu, D.S., Tajbakhsh, S., Kelly, R.G., Wernig, A., Buckingham, M.E., Partridge, T.A., and Zammit, P.S. (2000). Expression of CD34 and Myf5 defines the majority of quiescent adult skeletal muscle satellite cells. J. Cell Biol. *151*, 1221–1234.

Biressi, S., Molinaro, M., and Cossu, G. (2007). Cellular heterogeneity during vertebrate skeletal muscle development. Dev. Biol. *308*, 281–293.

Bowman, G.R., Comolli, L.R., Zhu, J., Eckart, M., Koenig, M., Downing, K.H., Moerner, W.E., Earnest, T., and Shapiro, L. (2008). A polymeric protein anchors the chromosomal origin/ParB complex at a bacterial cell pole. Cell *134*, 945–955.

Cairns, J. (1975). Mutation selection and the natural history of cancer. Nature *255*, 197–200.

Cairns, J. (2006). Cancer and the immortal strand hypothesis. Genetics *174*, 1069–1072.

Collins, C.A., Olsen, I., Zammit, P.S., Heslop, L., Petrie, A., Partridge, T.A., and Morgan, J.E. (2005). Stem cell function, self-renewal, and behavioral heterogeneity of cells from the adult muscle satellite cell niche. Cell *122*, 289–301.

Conboy, M.J., Karasov, A.O., and Rando, T.A. (2007). High incidence of non-random template strand segregation and asymmetric fate determination in dividing stem cells and their progeny. PLoS Biol. *5*, e102.

Cortés, F., Pastor, N., Mateos, S., and Domínguez, I. (2003). The nature of DNA plays a role in chromosome segregation: endoreduplication in halogen-substituted chromosomes. DNA Repair (Amst.) *2*, 719–726.

DePrimo, S.E., Stambrook, P.J., and Stringer, J.R. (1996). Human placental alkaline phosphatase as a histochemical marker of gene expression in transgenic mice. Transgenic Res. *5*, 459–466.

Escobar, M., Nicolas, P., Sangar, F., Laurent-Chabalier, S., Clair, P., Joubert, D., Jay, P., and Legraverend, C. (2011). Intestinal epithelial stem cells do not protect their genome by asymmetric chromosome segregation. Nat. Commun. *2*, 258.

Falconer, E., Chavez, E.A., Henderson, A., Poon, S.S., McKinney, S., Brown, L., Huntsman, D.G., and Lansdorp, P.M. (2010). Identification of sister chromatids by DNA template strand sequences. Nature *463*, 93–97.

Fuchs, E., Tumbar, T., and Guasch, G. (2004). Socializing with the neighbors: stem cells and their niche. Cell *116*, 769–778.

Garstka, H.L., Schmitt, W.E., Schultz, J., Sogl, B., Silakowski, B., Pérez-Martos, A., Montoya, J., and Wiesner, R.J. (2003). Import of mitochondrial transcription factor A (TFAM) into rat liver mitochondria stimulates transcription of mitochondrial DNA. Nucleic Acids Res. *31*, 5039–5047.

Gayraud-Morel, B., Chrétien, F., Flamant, P., Gomès, D., Zammit, P.S., and Tajbakhsh, S. (2007). A role for the myogenic determination gene Myf5 in adult regenerative myogenesis. Dev. Biol. *312*, 13–28.

Gayraud-Morel, B., Chrétien, F., and Tajbakhsh, S. (2009). Skeletal muscle as a paradigm for regenerative biology and medicine. Regen. Med. *4*, 293–319.

Hall, J.K., Banks, G.B., Chamberlain, J.S., and Olwin, B.B. (2010). Prevention of muscle aging by myofiber-associated satellite cell transplantation. Sci. Transl. Med. *2*, 57ra83.

Gayraud-Morel, B., Chrétien, F., Jory, A., Sambasivan, R., Negroni, E., Flamant, P., Soubigou, G., Coppée, J.-Y., Di Santo, J., Cumano, A., Mouly, V., and Tajbakhsh, S. (2012). Myf5 haploinsufficiency reveals distinct cell fate potentials for adult skeletal muscle stem cells. J. Cell Science.

Jory, A., Le Roux, I., Gayraud-Morel, B., Rocheteau, P., Cohen-Tannoudji, M., Cumano, A., and Tajbakhsh, S. (2009). Numb promotes an increase in skeletal muscle progenitor cells in the embryonic somite. Stem Cells *27*, 2769–2780.

Kelly, R., Alonso, S., Tajbakhsh, S., Cossu, G., and Buckingham, M. (1995). Myosin light chain 3F regulatory sequences confer regionalized cardiac and skeletal muscle expression in transgenic mice. J. Cell Biol. *129*, 383–396.

Kitamoto, T., and Hanaoka, K. (2010). Notch3 null mutation in mice causes muscle hyperplasia by repetitive muscle regeneration. Stem Cells *28*, 2205–2216.

Klar, A.J. (1994). A model for specification of the left-right axis in vertebrates. Trends Genet. *10*, 392–396.

Kuang, S., and Rudnicki, M.A. (2008). The emerging biology of satellite cells and their therapeutic potential. Trends Mol. Med. *14*, 82–91.

Kuang, S., Chargé, S.B., Seale, P., Huh, M., and Rudnicki, M.A. (2006). Distinct roles for Pax7 and Pax3 in adult regenerative myogenesis. J. Cell Biol. *172*, 103–113.

Kuang, S., Kuroda, K., Le Grand, F., and Rudnicki, M.A. (2007). Asymmetric self-renewal and commitment of satellite stem cells in muscle. Cell *129*, 999–1010.

Lansdorp, P.M. (2007). Immortal strands? Give me a break. Cell *129*, 1244–1247.

Lepper, C., Conway, S.J., and Fan, C.M. (2009). Adult satellite cells and embryonic muscle progenitors have distinct genetic requirements. Nature *460*, 627–631.

Li, L., and Clevers, H. (2010). Coexistence of quiescent and active adult stem cells in mammals. Science *327*, 542–545.

Macara, I.G., and Mili, S. (2008). Polarity and differential inheritance—universal attributes of life? Cell *135*, 801–812.

Mitchell, P.O., Mills, T., O'Connor, R.S., Kline, E.R., Graubert, T., Dzierzak, E., and Pavlath, G.K. (2005). Sca-1 negatively regulates proliferation and differentiation of muscle cells. Dev. Biol. *283*, 240–252.

Montarras, D., Morgan, J., Collins, C., Relaix, F., Zaffran, S., Cumano, A., Partridge, T., and Buckingham, M. (2005). Direct isolation of satellite cells for skeletal muscle regeneration. Science *309*, 2064–2067.

Moyes, C.D., and Battersby, B.J. (1998). Regulation of muscle mitochondrial design. J. Exp. Biol. *201*, 299–307.

Neumüller, R.A., and Knoblich, J.A. (2009). Dividing cellular asymmetry: asymmetric cell division and its implications for stem cells and cancer. Genes Dev. *23*, 2675–2699.

Oustanina, S., Hause, G., and Braun, T. (2004). Pax7 directs postnatal renewal and propagation of myogenic satellite cells but not their specification. EMBO J. *23*, 3430–3439.

Potten, C.S., Owen, G., and Booth, D. (2002). Intestinal stem cells protect their genome by selective segregation of template DNA strands. J. Cell Sci. *115*, 2381–2388.

Quyn, A.J., Appleton, P.L., Carey, F.A., Steele, R.J., Barker, N., Clevers, H., Ridgway, R.A., Sansom, O.J., and Näthke, I.S. (2010). Spindle orientation bias in gut epithelial stem cell compartments is lost in precancerous tissue. Cell Stem Cell *6*, 175–181.

Rando, T.A. (2007). The immortal strand hypothesis: segregation and reconstruction. Cell *129*, 1239–1243.

Relaix, F., Montarras, D., Zaffran, S., Gayraud-Morel, B., Rocancourt, D., Tajbakhsh, S., Mansouri, A., Cumano, A., and Buckingham, M. (2006). Pax3 and Pax7 have distinct and overlapping functions in adult muscle progenitor cells. J. Cell Biol. *172*, 91–102.

Sacco, A., Doyonnas, R., Kraft, P., Vitorovic, S., and Blau, H.M. (2008). Self-renewal and expansion of single transplanted muscle stem cells. Nature *456*, 502–506.

Sambasivan, R., Gayraud-Morel, B., Dumas, G., Cimper, C., Paisant, S., Kelly, R.G., and Tajbakhsh, S. (2009). Distinct regulatory cascades govern extraocular and pharyngeal arch muscle progenitor cell fates. Dev. Cell *16*, 810–821.

Sambasivan, R., Yao, R., Kissenpfennig, A., Van Wittenberghe, L., Paldi, A., Gayraud-Morel, B., Guenou, H., Malissen, B., Tajbakhsh, S., and Galy, A. (2011). Pax7-expressing satellite cells are indispensable for adult skeletal muscle regeneration. Development *138*, 3647–3656.

Schepers, A.G., Vries, R., van den Born, M., van de Wetering, M., and Clevers, H. (2011). Lgr5 intestinal stem cells have high telomerase activity and randomly segregate their chromosomes. EMBO J. *30*, 1104–1109.

Seale, P., Sabourin, L.A., Girgis-Gabardo, A., Mansouri, A., Gruss, P., and Rudnicki, M.A. (2000). Pax7 is required for the specification of myogenic satellite cells. Cell *102*, 777–786.

Sherwood, R.I., Christensen, J.L., Conboy, I.M., Conboy, M.J., Rando, T.A., Weissman, I.L., and Wagers, A.J. (2004). Isolation of adult mouse myogenic progenitors: functional heterogeneity of cells within and engrafting skeletal muscle. Cell *119*, 543–554.

Shinin, V., Gayraud-Morel, B., Gomès, D., and Tajbakhsh, S. (2006). Asymmetric division and cosegregation of template DNA strands in adult muscle satellite cells. Nat. Cell Biol. *8*, 677–687.

Tajbakhsh, S. (2008). Stem cell identity and template DNA strand segregation. Curr. Opin. Cell Biol. *20*, 716–722.

Tajbakhsh, S. (2009). Skeletal muscle stem cells in developmental versus regenerative myogenesis. J. Intern. Med. *266*, 372–389.

Tajbakhsh, S., and Gonzalez, C. (2009). Biased segregation of DNA and centrosomes: moving together or drifting apart? Nat. Rev. Mol. Cell Biol. *10*, 804–810.

White, M.A., Eykelenboom, J.K., Lopez-Vernaza, M.A., Wilson, E., and Leach, D.R. (2008). Non-random segregation of sister chromosomes in *Escherichia coli*. Nature *455*, 1248–1250.

Wilson, A., Laurenti, E., Oser, G., van der Wath, R.C., Blanco-Bose, W., Jaworski, M., Offner, S., Dunant, C.F., Eshkind, L., Bockamp, E., et al. (2008). Hematopoietic stem cells reversibly switch from dormancy to self-renewal during homeostasis and repair. Cell *135*, 1118–1129.

Zammit, P.S., Golding, J.P., Nagata, Y., Hudon, V., Partridge, T.A., and Beauchamp, J.R. (2004). Muscle satellite cells adopt divergent fates: a mechanism for self-renewal? J. Cell Biol. *166*, 347–357.

Zammit, P.S., Partridge, T.A., and Yablonka-Reuveni, Z. (2006). The skeletal muscle satellite cell: the stem cell that came in from the cold. J. Histochem. Cytochem. *54*, 1177–1191.